Effect of parameters-dependent viscosity and thermal conductivity on the thermo-hydraulic performance of Al_2O_3-based nanofluids in a rectangular microchannel

Hongyan HUANG[1, 2], Chunquan LI[1, 2*], Yuling SHANG[3], Siyuan HUANG[1]

[*1]School of Mechanical and Electrical Engineering, Guilin University of Electronic Technolgy, China

[2]Guangxi Key Lab of Manufacturing System Advanced Manufacturing Technology, China

[3]School of Electronic Engineering and Automation, Guilin University of Electronic and Technology, Guilin, 541004, China

* Corresponding author: E-mail: lcq@guet.edu.cn

Abstract: The multi-parameter dependence of nanofluid viscosity and thermal conductivity on the flow and heat transmission properties of Al_2O_3-H_2O nanofluid in microchannels is investigated in this paper using a numerical simulation approach, exploring the effects of various parameters on flow and heat dissipation characteristics, such as flow velocity, pressure drop, temperature, and heat transfer coefficient, under different Reynolds numbers, etc. These parameters include the nanoparticle sphericity (0.5~1.0), volume fraction (0.6%~6.0%), and temperature (290K~370K) of the nanofluids, as well as the boundary parameter Reynolds number (200~1000). The results show that the multi-parameter dependence of nanofluid viscosity and thermal conductivity setting has a significant impact on the flow and heat dissipation characteristics of nanofluids, comparing analysis with the nanofluid viscosity and thermal conductivity only related to the volume fraction under the same condition. Under the combined action of sphericity, volume fraction, and temperature, increasing the sphericity increases the pressure drop and decreases the heat transfer coefficient. For example, at a Reynolds number of 1000, the maximum rates of change for pressure drop and heat transfer coefficient are 0.85 and 4.26, respectively. The nanofluid thermo-hydraulic performance is sensitive to temperature, volume fraction and sphericity in turn. Setting up viscosity and thermal conductivity equations with multiple parameter dependencies can provide more accurate results for the research of nanofluids, further deepening the application research of nanofluids.

Keywords: multi-parameter dependence of nanofluid viscosity and thermal conductivity; Al_2O_3-H_2O nanofluid; comparing analysis; Sensitive

1. Introduction

Nanofluids have been widely applied in various engineering fields, particularly in energy and power, aerospace, biochemical engineering, nuclear, and microelectronics, due to their excellent thermal conductivity[1-3], and have also drawn more attention from researchers[4-6]. The viscosity and thermal conductivity of nanofluids significantly influence their flow and heat transfer characteristics, and different constitutive equations sometimes exhibit significant differences[7-9]. This work contributes to a deeper understanding of the use of nanofluids in heat and mass transfer by examining the multi-parameter thermophysical dependence of nanofluids on their flow and heat dissipation

characteristics in microfluidic channels.

Lee et al.[10] investigated the viscosity of Al_2O_3 nanofluids in water and proposed a relationship between viscosity, temperature, and particle volume fraction. The viscosity significantly decreases with increasing temperature and increases with increasing volume fraction of alumina. Cong Tam Nguyen et al.[11] investigated the effects of temperature and particle size on the dynamic viscosity of two water-based mixtures, water-Al_2O_3 and water-CUO, using experimental methods. They found that when the particle volume fraction was less than 4%, the viscosity of alumina-water nanofluids with particle sizes of 36 nm and 47 nm was approximately the same. However, for higher particle fractions, the viscosity of the 47 nm particle size was significantly higher than that of the 36 nm particle size. Davood Toghraie et al.[12] investigated the thermal conductivity of graphene oxide-al_2o_3/water-glycol hybrid nanofluids at different nanoparticle temperatures and volume fractions using artificial neural networks (ANN). The flow heat transfer characteristics of various mixed nanofluids (including water-based nanofluids containing aluminum trioxide) in different heat exchangers, such as microchannels, were studied using numerical methods. The goal was to determine the optimal heat dissipation structure or parameters and to obtain the changing law of temperature and Nussel number under each factor[13-16]. Ali J. Chamkha et al.[17, 18] investigated the combined effects of nanofluids, such as molybdenum disulfide nanofluids, under thermal, flow, and magnetic fields using computational methods to enhance heat exchanger performance in terms of heat transfer.

It is evident from the literature above that the primary parameters of volume fraction are the main focus of the viscosity and thermal conductivity models of nanofluids. Additionally, some models take into account the impacts of particle size parameters and volume fraction[19, 20], or the combined effects of temperature and volume fraction on fluid viscosity[21]. It is also taken into consideration how temperature and volume fraction affect thermal conductivity[22-24], as well as how volume fraction and particle size affect it[25-27]. Nevertheless, there may be variations in the associated analytical results because these models do not fully represent the multi-parameter dependency of viscosity and thermal conductivity in nanofluids.

This paper's goal is to examine how the flow and heat transfer properties of alumina nanofluids in microfluidic channels are influenced by their reliance on temperature, volume fraction, and particle sphericity. Finding the relationship between these variables and the heat transfer coefficient, pressure drop, and overall evaluation factor will be helpful in choosing appropriate nanofluids. These will support the use of nanofluids in microfluidic heat exchangers for improved heat dissipation.

2. Multiparameter dependence of viscosity and thermal conductivity of Al_2O_3-H_2O nanofluid

In this paper, the viscosity and thermal conductivity of nanofluids are modeled using Eq. (1) and Eq. (2)[28, 29], respectively, to examine the impact of the multiparameter dependence of these parameters on the flow and heat dissipation performance of the fluids in microfluidic channels. Figure 1 confirms the reliability of the viscosity and thermal conductivity equation by comparing them with experimental data, which has a maximum relative error of less than 11% and, therefore, can be used in the study of this paper. And the density and specific heat capacity of the nanofluid are expressed using Eq. (3) and Eq.(4)[17, 18].

$$\frac{\eta_{nf}}{\eta_f} \times 10^3 = 125.85\varphi + 2.67T + 29.09\alpha - 8.20\varphi^2 + 0.51\varphi T - 171.89\varphi\alpha - 192.10 \quad (1)$$

$$\frac{\lambda_{nf}}{\lambda_f} \times 10^3 = 127.87\varphi + 4.65T - 1558.46\alpha - 5.07\varphi^2 + 1265.95\alpha^2 - 3.46\alpha T - 33.96\alpha\varphi + 918.73 \quad (2)$$

$$\rho_{nf} = \rho_f(1-\varphi) + \rho_p \quad (3)$$

$$(\rho C_p)_{nf} = (\rho C_p)_f(1-\varphi) + (\rho C_p)_p\varphi \quad (4)$$

In the equation, η_{nf} represents the dynamic viscosity of alumina nanofluid, λ_{nf} represents the thermal conductivity of nanofluid, η_f represents the viscosity of the base fluid, and λ_f represents the thermal conductivity of the base fluid. And α represents the sphericity of nanoparticles, $\varphi(0.6\%\sim6.0\%)$ is the volume fraction of particles, and $T(290K\sim370K)$ represents the temperature of nanofluid.

Here, Eq. (5), which provides a full characterization of the various particle sizes and shapes, defines particle sphericity(α, 0.5~1.0), and a spherical particle has a sphericity of 1[30].

$$\alpha = \frac{S_V}{S_p} = \frac{4\pi\left(\frac{3V_F}{4\pi}\right)^{\frac{2}{3}}}{S_p} \quad (5)$$

Where, S_V is the surface area of a sphere of the same volume as the particle, V_F is the particle volume, and S_p is the particle surface area, α.is the particle sphericity.

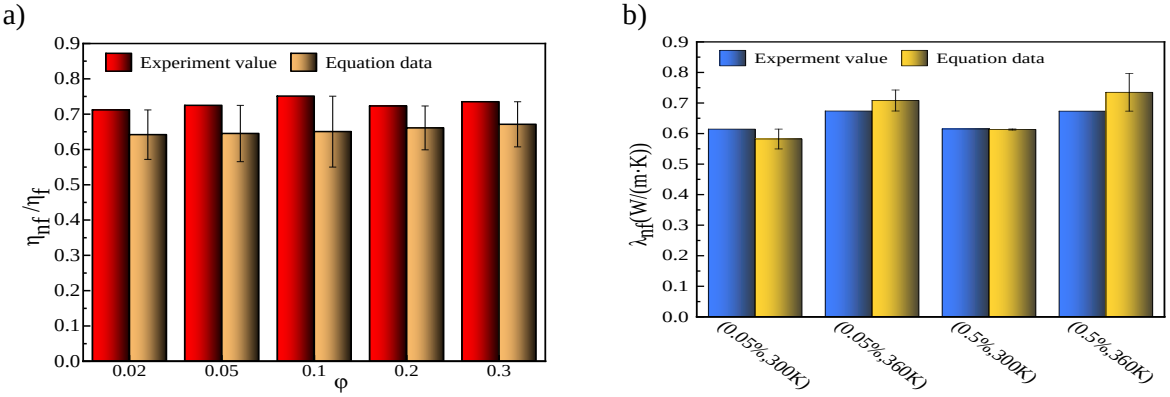

Figure 1 Validity of equations. a) Viscosity equation validation; b) Thermal conductivity equation validation

From the above equations, the viscosity and thermal conductivity of nanofluids are closely related to three parameters that must be considered in their use. In particular, the viscosity and thermal conductivity of the nanofluid largely determine its flow and heat transfer characteristics in the microchannel. Therefore, when studying the flow and heat transfer properties of nanofluids, the influence of the multi-dimensional parametric dependence of viscosity and thermal conductivity must be considered. Further elaboration is provided in subsequent studies.

3. Numerical simulation

3.1 Computational model

To ensure the accuracy of the ensuing analytical procedure and outcomes, a numerical

simulation model has been created in this part using the software COMSOL and calibrated. Gridded microfluidic heat sinks generally consist of two main flow channels and several auxiliary flow channels. Therefore, full-domain simulations are expensive in terms of time and CPU usage. In the current study, the heat transfer heat of flow of the nanofluid occurs only between the fluid and the solid, so the symmetry and scalability of the numerical analysis of the microfluidic unit can be exploited by using an aluminum-based unit microfluidic channel with a length of 10 mm, a height of 500 μm and a width of 200 μm. The model schematic is shown in Figure 2 and its specific dimensional parameters are shown in Table 1.

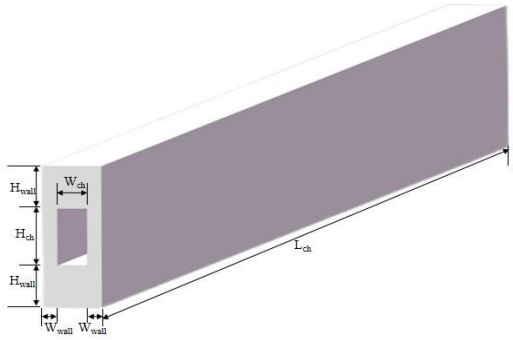

Figure 2 Schematic of the rectangular heat sink unit cell

Table 1 Dimensions of the rectangular shape microchannel heat sink unit cell

L_{ch}(mm)	H_{ch}(μm)	W_{ch}(μm)	H_{wall}(μm)	W_{wall}(μm)
10	200	100	150	50

The following assumptions are considered to simplify the simulation:

1. Nanofluid is considered steady, incompressible, and laminar, following the Hagen-Poiseuille equation.
2. Negligible gravity and boundary slip.
3. Thermal conductivity and viscosity of nanofluids are determined by personalized parameters-dependent models.

The simulations are performed with the commercial software COMSOL Multiphysics 6.1, where the uniform velocity is applied at the channel inlet and the pressure outlet condition is assigned to the channel outlet with velocity-pressure coupling. Nanofluids in microfluidic channels still follow the conservation of mass continuity, moment, and energy as the set of governing equations Eq. (6). To better minimize the interference of other factors with the heat transfer performance of the nanofluid flow in the microfluidic channel, a uniform heat flux is applied to the upper surface and the other surfaces are adiabatic.

$$\begin{aligned} \nabla u &= 0 \\ \varrho(\mathrm{u}\cdot\nabla\mathrm{u}) &= -\nabla \mathrm{p} + \mu^2\nabla\mathrm{u} \\ \varrho\nabla(\mathrm{u}) &= 0 \end{aligned} \tag{6}$$

The specific boundary setting can be expressed as a system of equations as follows[18, 31-35]:

In the fluid domain,

$$x = 0, u = u_{in}, v = w = 0, T = T_{in} \tag{7}$$

$$x = L_{ch}, \frac{\partial u}{\partial x} = \frac{\partial v}{\partial x} = \frac{\partial w}{\partial x} = 0, p = p_{out} \quad (8)$$

At the top of the microchannel is uniform heat flux,

$$z = H_{wall} + H_{ch}, -\lambda_s \frac{\partial T}{\partial z} = q_w^{\leftrightarrow} \quad (9)$$

At the bottom of the microchannel is an adiabatic condition,

$$z = 0, \frac{\partial T}{\partial z} = 0 \quad (10)$$

$$y = 0 \; and \; y = W_{wall} + W_{ch}, \frac{\partial T}{\partial y} = 0 \quad (11)$$

3.2 Mesh independence

Good mesh quality can help ensure the accuracy and stability of simulation results, and also, improve the speed and convergence of calculations. Four different grid models were used for the calculations and the comparison revealed that all three metrics used to evaluate the quality of the grid remained very stable when the number of grid cells reached around 636,000, as shown in Table 2. The grid skewness gets closer to 1 as the number of cells increases, but the growth becomes very slow; the pressure energy done by the fluid and the average fluid temperature(Tav) change is negligible. Therefore, taking into account computational efficiency, numerical reliability and cost, Further processing was done using this grid layout, which has 635724 elements.

Table 2 Grid independence test for model.

Elements number	Skewness	Skewness -difference	Pressure Energy（J）	Pressure Energy -difference	T_{av}（K）	T_{av} -difference
89713	0.6307	reference	1.29E-06	reference	311.22	reference
204077	0.6556	3.95%	1.30E-06	0.82%	309.42	0.58%
635724	0.6638	1.25%	1.30E-06	0.00%	306.76	0.86%
2518194	0.6717	1.19%	1.30E-06	0.00%	306.76	0.00%

3.3 Method verification

To further validate the numerical model and simulation method, the structure from the literature [36] is adopted. A comparison of the results is shown in Figure 3, which shows a good match between the literature results and the simulation results. Not only is the trend of fluid pressure drop and inlet/outlet temperature difference with Reynolds number consistent, but the errors in both indicators are small, with a relative error of less than 10% for most data.

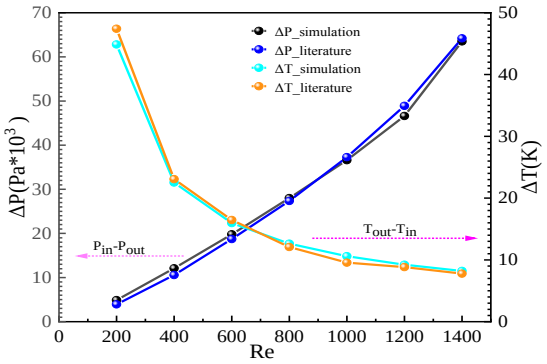

Figure 3 Validation of numerical model

4. Data reductions

This section explains the main formulas used in the analysis of data obtained from numerical simulations. The pressure drop Δp is characterized as the difference between the average pressure on the inlet and outlet surfaces and the temperature difference ΔT is the difference in the average surface temperature between the outlet and the inlet.

Where, x is the microfluidic axial coordinate, μ and ρ is the average dynamic viscosity and density in the cross-section at x, and v_∞ is the maximum velocity in the cross-section at x.

The expression for the average friction coefficient(f) of nanofluid in the microchannel is

$$f = \frac{2\,\Delta p D_{\mathrm{h}}}{\rho_{\mathrm{av}} L_{\mathrm{ch}} u_{x\mathrm{av}^2}} \tag{12}$$

Where, ρ_{av} is the nanofluid average density over the entire fluid domain(Ωmch), $u_{x\mathrm{av}}$ is the nanofluid average velocity along the x-direction, D_{h} is the hydraulic diameter of the microchannel expressed as Eq. (13).

$$D_{\mathrm{h}} = \frac{2H_{\mathrm{ch}}W_{\mathrm{ch}}}{H_{\mathrm{ch}} + W_{\mathrm{ch}}} \tag{13}$$

The average heat transfer coefficient(h_{av}) reflects the convective heat exchange capacity between the nanofluid and the solid wall surface in the microfluidic channel with the following formula:

$$h_{av} = \frac{q_{\mathrm{w}} A_t}{A_{\mathrm{tot}}\left(T_{\mathrm{w}} - T_f\right)} \tag{14}$$

Here, A_t is the top wall near the heat source, A_{tot} is the four walls of the microfluidic channel, T_{w} is the average temperature on the surface A_t, and T_f is the mean temperature over the entire fluid domain(Ωmch).

5. Result and discussion

The discussion of the results of the analysis is fully developed in this section. The law of influence of multi-parameter effects of nanofluid viscosity and thermal conductivity on its flow heat transfer characteristics in microfluidic channel at different Reynolds numbers is obtained. A comparison analysis also reveals the need for carrying out a multiparameter dependence investigation of the thermophysical characteristics of nanofluids. In this paper, the results are also analyzed in comparison

with the results of associating only the volume fraction in the physical property equations of viscosity and thermal conductivity under the same conditions, which use the viscosity and thermal conductivity expressions as Eq. (15) [37]and (16)[38].

$$\mu_{nf} = \mu_f(1 + 2.5\varphi) \tag{15}$$

$$\frac{k_{nf}}{k_f} = \frac{k_p + 2k_f + 2\varphi(k_f - k_p)}{k_p + 2k_f - \varphi(k_f - k_p)} \tag{16}$$

5.1 Effect of parameters on liquidity performance of Al_2O_3-H_2O nanofluid

1) Variation in nanofluid dynamic viscosity

Figure 4(a) exhibits a linear increase and the increase in dynamic viscosity decreases as the Reynolds number increases, and the rate of change of μ_{av} with α is almost equal for different Reynolds numbers. In the case of relatively slow flow, the effect of increased molecular spacing of the fluid temperature rise is lower than the increased inter-particle adsorption due to increased sphericity, leading to increased internal friction and increased μ_{av}. Figure 4(b) shows a wave-like upward growth pattern with the increase of volume fraction. It has a high dynamic viscosity at low Reynolds number and high volume fraction. This phenomenon may be because the increased inter-particle adsorption of increasing concentration outweighs the dilution effect of increasing temperature on viscosity, thus increasing the kinetic viscosity. For the same Reynolds number, the change in dynamic viscosity due to volume fraction is higher than that due to sphericity, the respective values are approximately 1.89 and 0.34. with Re=200. In Figure 4, the star points represent the data used for comparison, and it is found that the Reynolds number change does not affect the dynamic viscosity of the nanofluid. Moreover, the viscosity when considering only the volume fraction is skewed more than when combining the effects of temperature, volume fraction, and sphericity. Higher dynamic viscosity results in greater power consumption, so it is advisable to use relatively lower sphericity and volume fraction.

a) b)

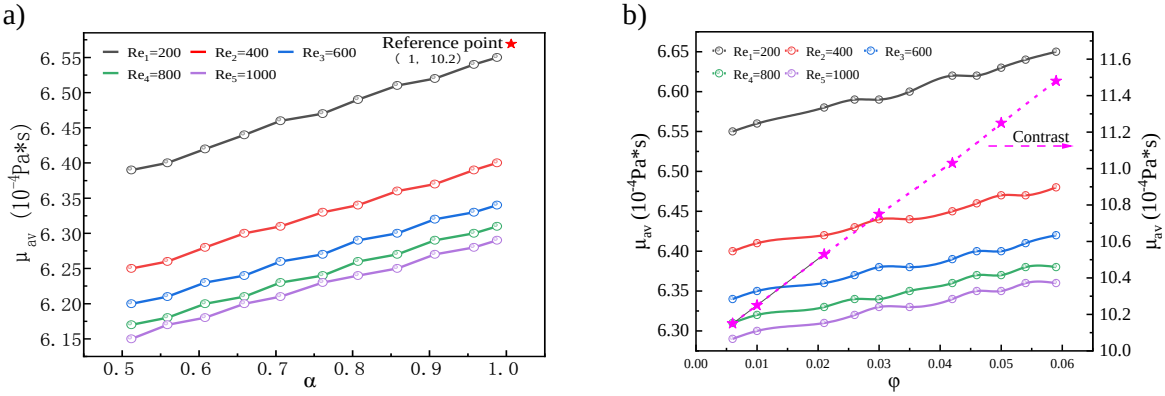

Figure 4 Variation in dynamic viscosity. a)Viscosity vs. sphericity; b) Viscosity vs. volume fraction

2) Velocity in nanofluid

Nanofluids primarily flow in microchannels under the influence of pressure and viscous forces, and variations in viscosity can result in velocity fluctuations. Here, selecting the transverse cross-section in the y-direction presents this phenomenon more intuitively.

In Figure 5(a) and (b), from the wall to the middle of the cross-section, the velocity is primarily

divided into two linear stages(approximately 27% and 28% of the semi-intercept interval, respectively.) as it approaches the mainstream velocity. It is observed that the rate of change in the first section is higher compared to the second section. For lower sphericity, it takes a longer time to reach the mainstream velocity. Additionally, the rate of velocity change in both sections increases with increasing sphericity. At a sphericity of 0.512, the rates are approximately k1=2.91 and k2=1.51, respectively. On the other hand, a lower volume fraction results in a closer approach to the mainstream velocity, and the rate of velocity change in both sections decreases with increasing volume fraction. At a volume fraction of 0.6%, the rates are approximately k1=2.98 and k2=1.54, respectively. When considering only the volume fraction (Figure 5 c), the velocity of the nanofluid reaches the main flow rate more directly from the near-wall end to the intermediate region instead of transitioning into two stages (Figure 5 a vs. Figure 5 b), as well as the larger fluctuation of the velocity due to the change of sphericity or the change of the volume fraction under the real-time temperature interaction. The faster the main flow rate is reached, the thinner the flow boundary layer along the axial direction of the flow channel becomes. This leads to an increased convective zone and enhances the convective heat dissipation effect of the nanofluid in the microfluidic channel. Therefore, it is recommended to use nanofluids with low concentration and high sphericity for improved convective heat dissipation.

a)

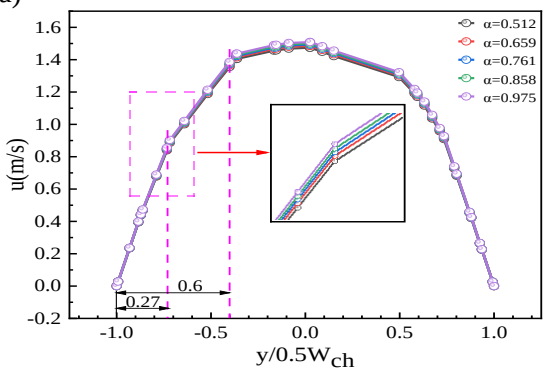

b)

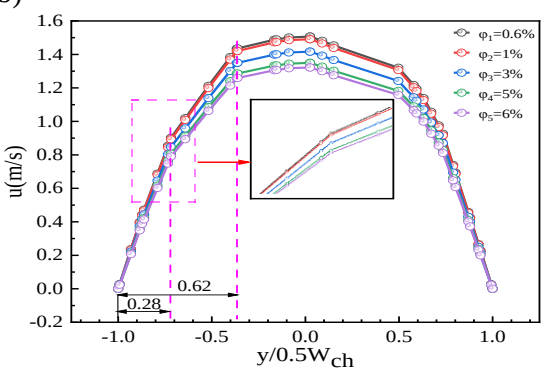

c)

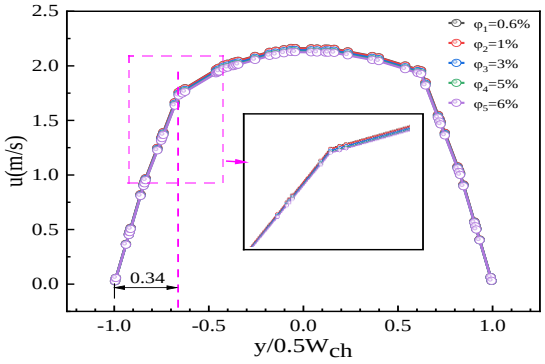

Figure 5 Variation of y-directional cross-sectional velocity at $Re_{in} = 200\ and\ x = L_{ch}/2$ a)Viscosity vs sphericity; b) Viscosity vs. volume fraction; c) Contrast chart (considering volume fractions only)

3) Pressure drop in nanofluid

Figure 6(a) demonstrates that the pressure drop increases nearly linearly with increasing sphericity at different Reynolds numbers, and the rate of increase is more pronounced at higher Reynolds numbers. For instance, at Re=1000, the growth rate is approximately 6.5 KPa per unit of

sphericity, and at higher sphericity values, the pressure drop is also greater. For example, at α=0.988, Δp=74.4 KPa. On the other hand, Figure 6(b) reveals that the pressure drop decreases nearly linearly with increasing volume concentration at different Reynolds numbers, and the rate of decrease is more significant at higher Reynolds numbers. For instance, at Re=1000, the growth rate is approximately 167.5 KPa per unit volume concentration, and at lower volume fractions, the pressure drop value is greater. For example, at φ=0.6%, Δp=74.3 KPa. An increase in flow rate reduces the viscous force effect, and this phenomenon is more prominent for the increase in viscosity due to an increase in volume fraction and sphericity. When considering only the volume fraction (Figure 6(c)), the pressure drop of the nanofluid rises faster and the rate of increase becomes larger as the Reynolds number increases, which is reduced in Figure 6(a) and (b) under the real-time temperature interaction. An increase in the differential pressure drop at the inlet and outlet leads to an increase in the pump work. Therefore, it is advisable to choose a nanofluid with low sphericity and high volume fraction.

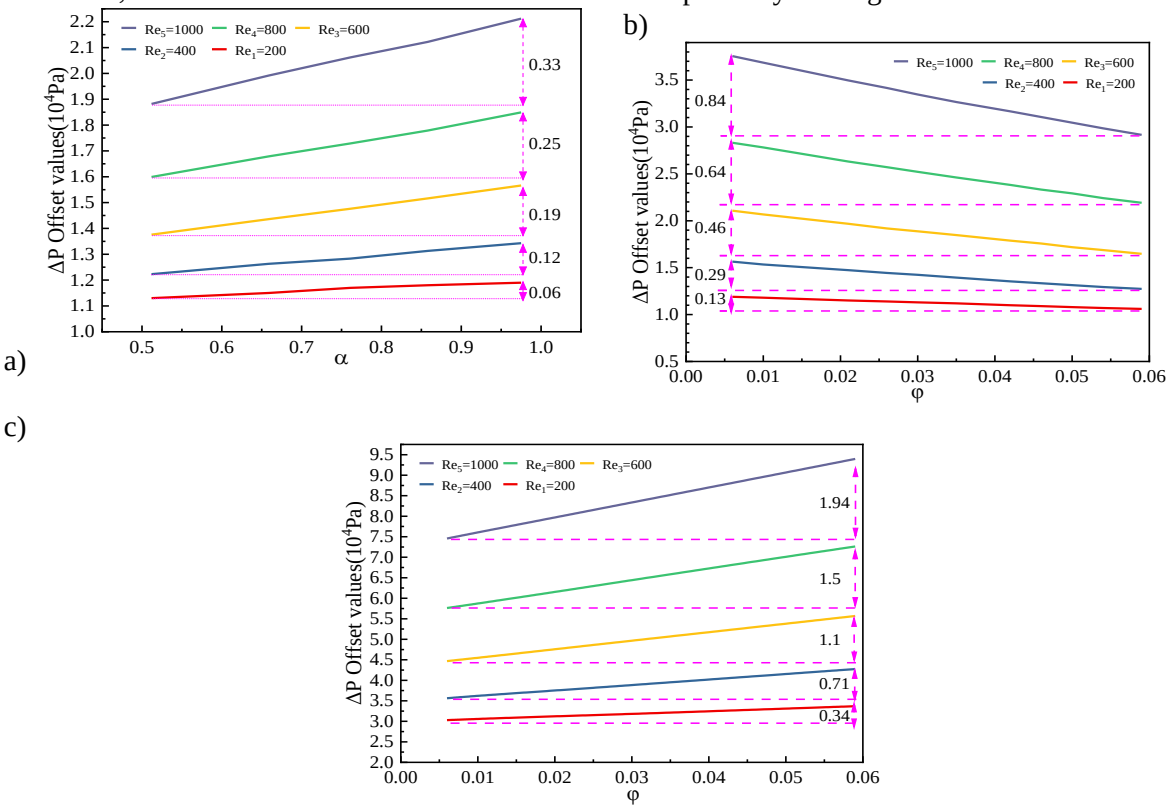

Figure 6 Variation of pressure drop. a)Pressure drop vs. sphericity; b) Pressure drop vs. volume fraction; c) Contrast chart (considering volume fractions only)

4) Variation in the thermal conductivity of nanofluids

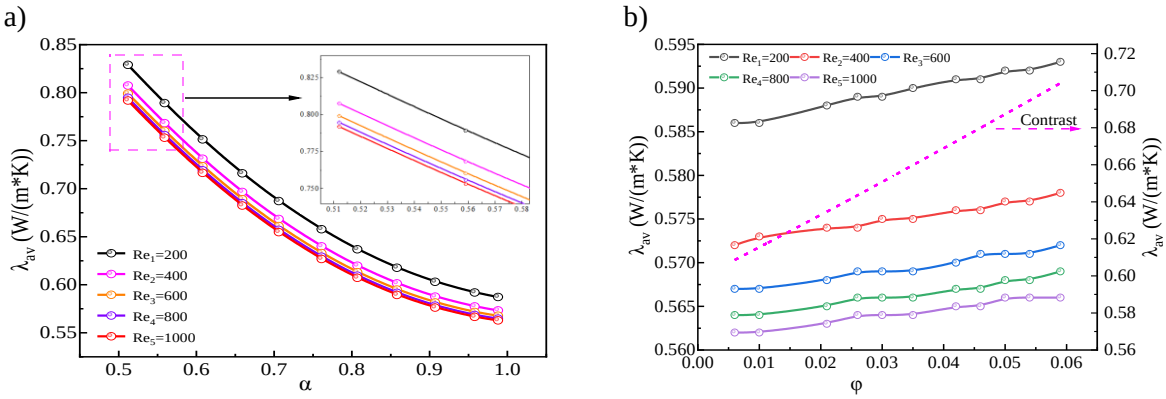

Figure 7 Variation in thermal conductivity. a) Thermal conductivity vs. sphericity; b) Thermal conductivity vs. volume fraction

Figure 7(a) shows that the thermal conductivity of the nanofluid decays exponentially with increasing sphericity, and the rate of reduction tends to slow down. The reason is that the increase in sphericity will reduce the contact area between the particles when they are close to spherical, reducing the heat transfer between them and leading to a decrease in thermal conductivity. At the same sphericity, lower Reynolds numbers have higher thermal conductivity, but increasing the Reynolds number, a decrease in thermal conductivity is observed, and this decrease tends to become smaller. For example, at α=0.512, the λ_{av} is 0.8289, 0.80741, 0.79909, 0.79462, 0.79181W/(m*K) for a change from R_e=200 to R_e=1000 respectively. Figure 7(b) shows a linear increase in the thermal conductivity of the nanofluid with increasing volume fraction. The reason is that an increase in particle concentration increases collisions between particles, intensifying the heat transfer between them and leading to an increase in thermal conductivity. Lower Reynolds numbers have higher thermal conductivity at the same volume fraction, but increasing the Reynolds number reveals a decrease in thermal conductivity, and this decrease tends to become smaller. For example, at φ=0.6%, the λ_{av} is 0.586, 0.572, 0.567, 0.564, 0.562W/(m*K) for a change from R_e =200 to R_e =1000 respectively. From Figure 7(b), only considering volume fraction (the dashed line in Figure b), the thermal conductivity increases linearly and the change of Reynolds number does not affect the rate of change. Under the combined effect of volume fraction and temperature, the thermal conductivity still increases, but the increase becomes smaller and fluctuates, and the growth rate is high at a low Reynolds number. Low sphericity and high volume concentration should be chosen to obtain higher thermal conductivity of the nanofluid.

5) Variation in the temperature of nanofluids

Figure 8 shows that an increase in both volume fraction and sphericity raises the average temperature of the fluid, but it varies as a power function of sphericity and tends to increase more slowly as sphericity approaches 1, and it varies linearly with volume fraction and the higher the volume fraction, the higher the temperature is. In Figure 8(a), the temperature is lower at low sphericity for the same Reynolds number, and the range of temperature change due to sphericity diminishes with increasing Reynolds number, and the rate of temperature rise also diminishes. If alpha goes from 0.512 to 0.988 and R_e goes from 200 to 1000, the corresponding temperature change ranges from 0.82 K to 0.12K, and the temperature rise rate at the starting point is from 2.34 to 0.34.

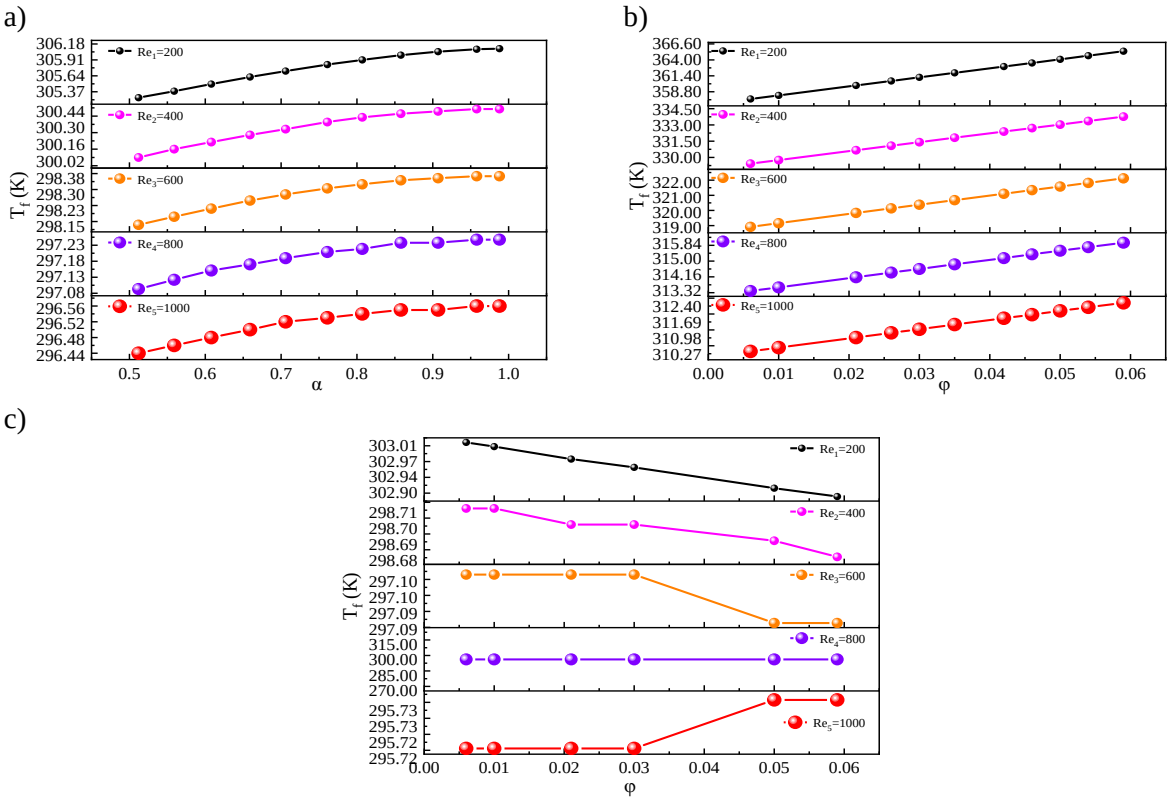

Figure 8 Variation in temperature. a) Temperature vs. sphericity; b) Temperature vs. volume fraction; c) Contrast chart (considering volume fractions only)

Also, Figure 8(b) shows that the temperature is higher at the same Reynolds number for higher volume fractions,and the range of temperature change and the temperature rise rate due to volume fraction both diminish with increasing Reynolds number. For example, for φ from 0.6% to 5.9% and Re from 200 to 1000, the corresponding temperature change range is from 7.8 K to 2.17 K, and the temperature rise rate from 146.75 to 41.0. A change in volume fraction leads to an even greater change in fluid temperature. The temperature decreases with the increase of volume fraction only taking the volume fraction (Figure 8(c)), but when the Reynolds number increases to 1000, the mobility is enhanced, and the particle concentration increases to a certain extent, which increases the temperature, i.e., the heat transfer effect of the nanofluid is enhanced. However, the volume fraction, sphericity and temperature work together (Figure 8(a) and (b)), the heat transfer effect is better, and all of them show an enhanced trend. For better diffusion of heat through the fluid, higher sphericity and volume fractions should be chosen.

6) Variation of convection heat transfer coefficient

Figure 9(a) shows that at the same Reynolds number, the rate of decline of the heat transfer coefficient is large at low sphericity, the closer it is to 1, the flatter the rate of decline. e.g. $Re = 1000$, $\alpha = 0.519$ and α=0.907, the rate of decline is 5.19 and 2.0 respectively. At different Reynolds numbers, the rate of decline is nearly the same at the same sphericity, e.g. $\alpha = 0.761$, the rate of decline is all approximately equal to 3.99. Figure 9(b) tells that at the same Reynolds number, low volume concentrations have high heat transfer coefficients, e.g. h_{av}= 12.26 for Re = 1000 and φ = 0..6%. The rate of decline becomes faster with increasing

Reynolds numbers.

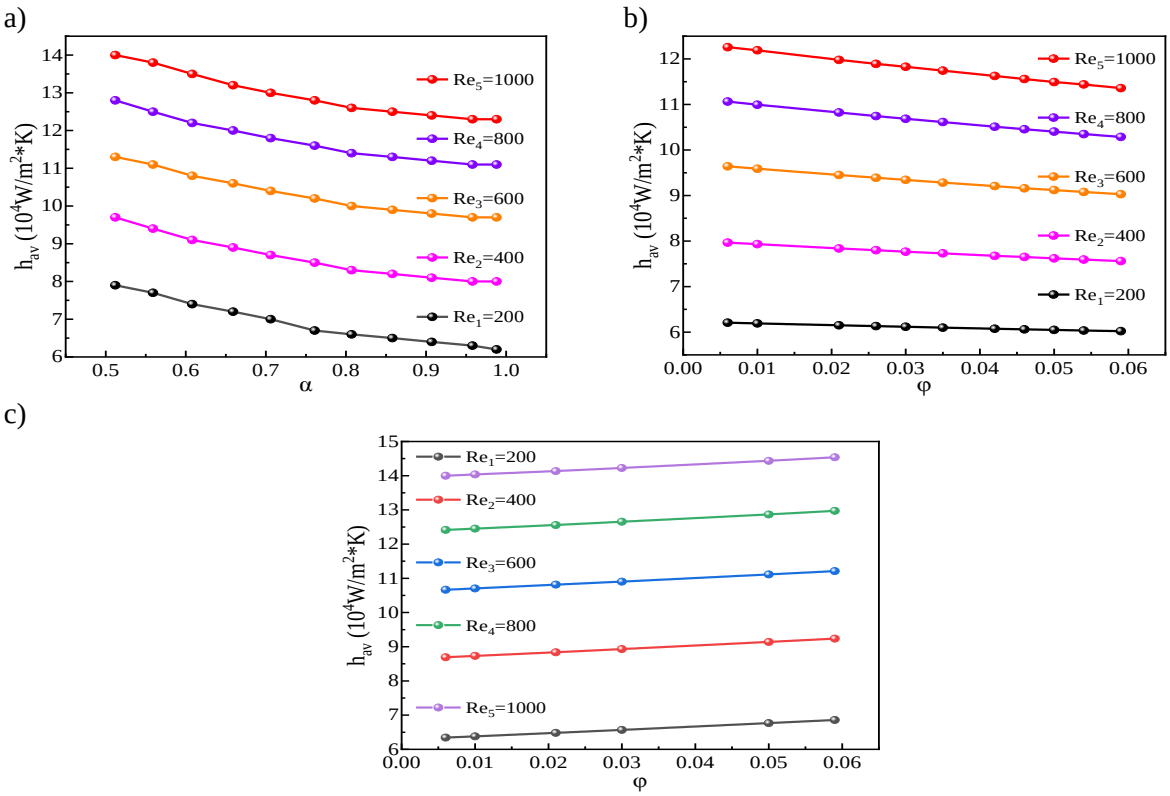

Figure 9 Variation in heat transfer coefficient. a) Coefficient vs. sphericity; b) Coefficient vs. volume fraction; c) Contrast chart (considering volume fractions only)

Volume fraction is solely considered (Figure 9(c)), the heat transfer coefficient increases with the increase of volume fraction, and the growth rate is almost equal at different Reynolds numbers. However, under the combined effect of volume fraction, sphericity and temperature (Figure 9(a) and Figure 9(b)), the sphericity and volume fraction leads to nonlinear and linear changes respectively. As sphericity and volume fraction increase, the frequency of collisions between fluid molecules and the wall decreases, leading to a reduction in the efficiency of heat exchange. Consequently, the heat exchange coefficient decreases as sphericity and volume fraction increase at the walls near the hot end. So, Small sphericity and low concentration of nanofluid should be chosen to improve the heat transfer effect.

5.2 Comprehensive evaluation factor analysis

Here, the effect of sphericity and volume concentration, temperature and their sensitivity to Reynolds number are further analyzed using a comprehensive evaluation factor η. η is expressed as shown in Eq.(17), with higher values reflecting enhanced heat transfer and lower resistance increases.

$$j = \frac{Nu}{Re \cdot Pr^{1/3}} = \frac{Nu}{Re \cdot \left(\frac{C_p \mu}{\lambda}\right)^{1/3}}, \eta = j/f \tag{17}$$

where η is the overall evaluation factor, characterizing the heat dissipation capacity of the nanofluid at low energy consumption; j is the heat dissipation capacity factor, characterizing the heat dissipation capacity of the fluid.

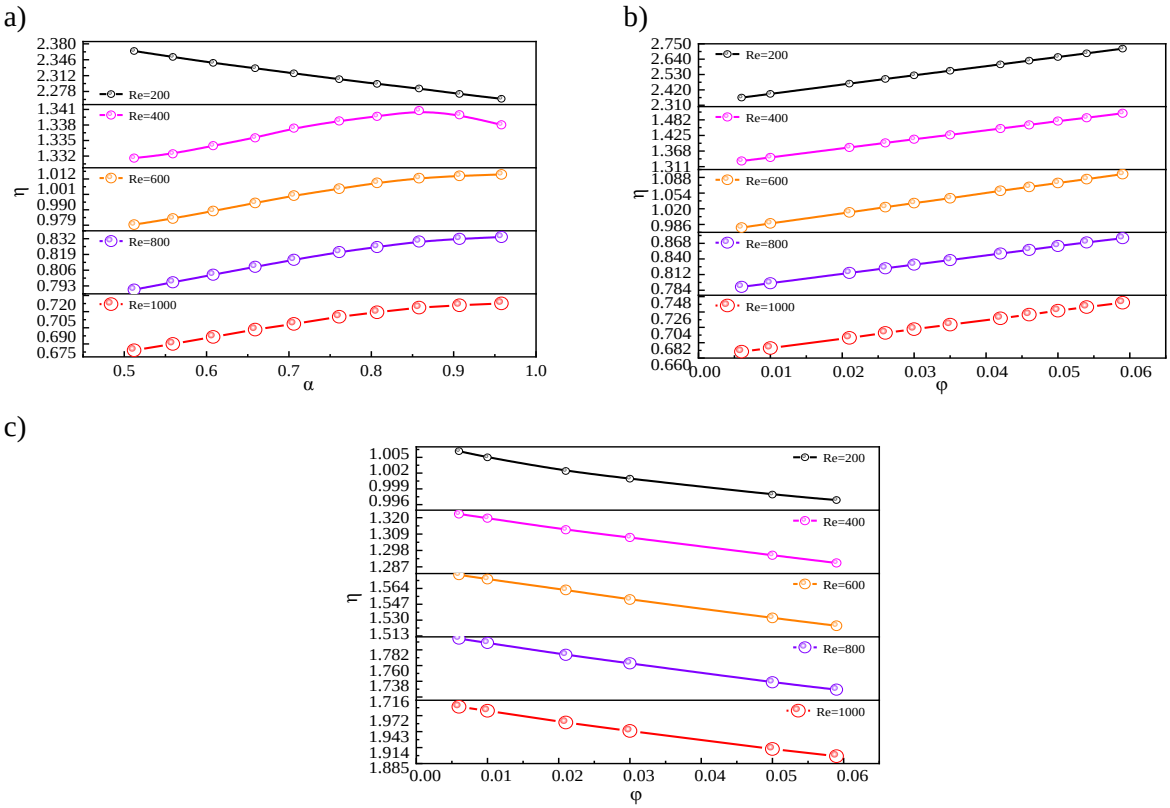

Figure 10 Integrated evaluation factor(η)variation. a) η vs sphericity; b) η vs volume fraction

Figure 10(a) shows that as the sphericity increases, at Re=200, η decreases approximately linearly, at Re=400, η first increases non-linearly, then α reaches 0.858 and then begins to decrease again; at Re=600-1000, η increases non-linearly in all cases, and the trend increases very slowly after α reaches 0.858. Figure 10(b) shows that at different Reynolds numbers, η increases linearly with increasing volume fraction, and the higher the Reynolds number, the smaller the rate of rise of η is. For example, at Re=200 and 1000, the rate of rise is 6.54 and 1.33 respectively. At the same sphericity, high volume fraction and low Reynolds number have high η, e.g. at φ=5.9%, Re=200 and 1000, the η values are 2.72 and 0.74 respectively. Only considering the volume fraction (Figure 10(c)), η decreases with the increase of the volume fraction, and the larger the Reynolds number, the faster the deceleration is. Under the joint effect of volume fraction, sphericity and temperature (Figure 10(a) and (b), η shows a general trend of growth. High volume fractions and sphericity should be taken at Reynolds numbers (≥ 400) to obtain high η.

6. Conclusions

This study analyzes the influence of the multi-variable dependence of nanofluid viscosity and thermal conductivity on the flow and heat transfer characteristics in microchannels with particle sphericity, volume fraction, and latent variable temperature. Some main conclusions are as follows:

1) Taking into account the dependence of thermophysical parameters on temperature, sphericity, and volume fraction would yield more dependable results and conclusions for nanofluid research.

2) The sensitivity indicators for Al_2O_3-H_2O nanofluids thermo-hydraulic performance are temperature, volume fraction and sphericity in turn.

3) At low Reynolds, the effect of the nanofluid-enhanced heat transfer will be better when temperature, sphericity, and volume fraction are combined. For example, Low sphericity and large volume fraction will improve the nanofluid's integrated thermal performance evaluation factor η to 2.75 at Reynolds number Re = 200 and volume fraction $\varphi = 0.6\%$.

4) The flow velocity from the near-wall end to the middle area of the channel is divided into two stages of transition under the combined impact of temperature, sphericity, and volume fraction.

5) The combined effects of temperature, sphericity, and volume fraction significantly reduce the difference in pressure drop between the flow channel's inlet and outlet. Additionally, the rate at which the pressure drop varies with parameter change is reduced in comparison to solely taking the volume fraction into account.

Nomenclature:

T	Temperature, K	Δp	inlet and outlet pressure drop
φ	Volume percent, vol%	η_f	Base fluid viscosity, Pa · s
α	particle sphericityW/m · k	η_{nf}	Nanofluid viscosity, Pa · s
μ_s	Shear viscosity, Pa · s	η_{nf}/η_f	Relative viscosity
μ_{bf}	Base fluid viscosity, Pa · s	V_F	Particle volume, m^3
L	Particle length, Å	S_P	Particle surface area, m^2
λ_{nf}	Nanofluid thermal conductivity, $W/m \cdot K$	L_{ch}	Length of microchannel, mm
λ_f	Base fluid thermal conductivity, $W/m \cdot K$	H_{ch}	Height of microchannel, μm
λ_{nf}/λ_f	Relative thermal conductivity	W_{ch}	Width of microchannel, μm
T_{nf}	the average fluid temperature of nanofluid, K	H_{wall}	Wall thickness in the height direction of microchannel, μm
λ_{av}	the average thermal conductivity of nanofluid, $W/m \cdot K$	W_{wall}	Wall thickness in the width direction of microchannel, μm
μ_{av}	the average dynamic viscosity of nanofluid, Pa · s	η	the overall evaluation factor
h_{av}	the convection heat transfer coefficient,$W/m^2 \cdot K$	η	the overall evaluation factor
j	the heat dissipation capacity factor	f	the friction coefficient

Acknowledgments： This work is supported by the National Natural Science Foundation of China (Nos.61661013, 51465013).

References:

[1] Mugilan, T., et al., The Use Of Smart Material Of Nanofluid For Heat Transfer Enhancement In Microtube With Helically Spiral Rib And Groove, Adv. Res. Mater. Sci., 32 (2017), pp. 1-12

[2] Ny, G.Y., et al., Numerical Study On Turbulent-Forced Convective Heat Transfer Of Ag/Heg Water Nanofluid In Pipe, Adv. Res. Mater. Sci., 22 (2016), pp. 11-27

[3] Baru, P.A., et al., Effect Of Viscous And Thermal Forcings On Dynamical Features Of Swimming Of Microorganisms In Nanofluids, J. Adv.Res. Fluid Mech. Therm. Sci., 17 (2016), pp. 18-27

[4] Sidik, N.A.C., Alawi, O.A., Computational Investigations On Heat Transfer Enhancement Using Nanorefrigerants, J. Adv. Res. Design., 1 (2014), pp. 35-41

[5] Baru, P.A., Lee, Y.K., The Use Of Nanofluids In Domestic Water Heat Exchanger, J. Adv. Res. Design., 3 (2014), pp. 9-24

[6] Trisaksri, V., Wongwises, S., Critical Review Of Heat Transfer Characteristics Of Nanofluids, Renewable & Sustainable Energy Reviews, 11 (2007), 3, pp. 512-523

[7] Koo, J., Computational nanofluid flow and heat transfer analyses applied to micro-systems, Proceedings, 2005

[8] Chan, H.C., et al., Empirical Correlation Finding The Role Of Temperature And Particle Size For Nanofluid (Al2O3) Thermal Conductivity Enhancement, Applied Physics Letters, 87 (2005), 15, pp. 435

[9] Mintsa, H.A., et al., New Temperature Dependent Thermal Conductivity Data For Water-Based Nanofluids, International Journal of Thermal Sciences, 48 (2009), pp. 363-371

[10] Lee, J.H., et al., Effective Viscosities And Thermal Conductivities Of Aqueous Nanofluids Containing Low Volume Concentrations Of Al2O3 Nanoparticles, International Journal of Heat and Mass Transfer, 51 (2008), 11-12, pp. 2651-2656

[11] Nguyen, C.T., et al., Temperature And Particle-Size Dependent Viscosity Data For Water-Based Nanofluids : Hysteresis Phenomenon, International Journal of Heat and Fluid Flow, 28 (2007), pp. 1492-1506

[12] Tian, S., et al., Using Perceptron Feed-Forward Artificial Neural Network (ANN) For Predicting The Thermal Conductivity Of Graphene Oxide-Al2O3/Water-Ethylene Glycol Hybrid Nanofluid, Case Studies in Thermal Engineering, 26 (2021), pp. 101055

[13] Khodabandeh, E., et al., Thermal Performance Improvement In Water Nanofluid/GNP–SDBS In Novel Design Of Double-Layer Microchannel Heat Sink With Sinusoidal Cavities And Rectangular Ribs, Journal of Thermal Analysis and Calorimetry, 136 (2018), pp. 1333-1345

[14] Barnoon, P., et al., Two Phase Natural Convection And Thermal Radiation Of Non-Newtonian Nanofluid In A Porous Cavity Considering Inclined Cavity And Size Of Inside Cylinders, International Communications in Heat and Mass Transfer, (2019)

[15] He, W., et al., Hydrothermal Performance Of Nanofluid Flow In A Sinusoidal Double Layer Microchannel In Order To Geometric Optimization, International Communications in Heat and Mass Transfer, (2020)

[16] Arasteh, H., et al., Heat Transfer Enhancement In A Counter-Flow Sinusoidal Parallel-Plate Heat Exchanger Partially Filled With Porous Media Using Metal Foam In The Channels' Divergent Sections, Journal of Thermal Analysis and Calorimetry, 141 (2019), pp. 1669-1685

[17] Raza, J., et al., Magnetohydrodynamic Flow Of Molybdenum Disulfide Nanofluid In A Channel With Shape Effects, Multidiscipline Modeling in Materials and Structures, (2019)

[18] Selimefendigil, F., et al., Role Of Magnetic Field On Forced Convection Of Nanofluid In A Branching Channel, International Journal of Numerical Methods for Heat & Fluid Flow, (2019)

[19] Gaganpreet, Srivastava, S., Viscosity Of Nanofluids: Particle Shape And Fractal Aggregates, Physics and Chemistry of Liquids, 53 (2015), pp. 174-186

[20] Fang, X., et al., Effects Of Inclusion Size On Thermal Conductivity And Rheological Behavior Of Ethylene Glycol-Based Suspensions Containing Silver Nanowires With Various Specific Surface Areas, International Journal of Heat and Mass Transfer, 81 (2015), pp. 554-562

[21] Hamid, K.A., et al., Investigation Of Al2O3 Nanofluid Viscosity For Different Water/EG Mixture Based, Energy Procedia, 79 (2015), pp. 354-359

[22] Kole, M., Dey, T.K., Thermal Conductivity And Viscosity Of Al2O3 Nanofluid Based On Car Engine Coolant, Journal of Physics D: Applied Physics, 43 (2010), pp. 315501

[23] Sundar, L.S., et al., Experimental Thermal Conductivity Of Ethylene Glycol And Water Mixture Based Low Volume Concentration Of Al2O3 And CuO Nanofluids, International Communications in Heat and Mass Transfer, 41 (2013), pp. 41-46

[24] Li, C.H., Peterson, G.P., Experimental Investigation Of Temperature And Volume Fraction Variations On The Effective Thermal Conductivity Of Nanoparticle Suspensions (Nanofluids), Journal of Applied Physics, 99 (2006), pp. 084314

[25] Mintsa, H.A., et al., New Temperature Dependent Thermal Conductivity Data For Water-Based Nanofluids, International Journal of Thermal Sciences, 48 (2009), pp. 363-371

[26] Bushehri, M.K., et al., Prediction Of Thermal Conductivity And Viscosity Of Nanofluids By Molecular Dynamics Simulation, Journal of Engineering Thermophysics, 25 (2016), pp.

389-400

[27] Beck, M.P., et al., The Effect Of Particle Size On The Thermal Conductivity Of Alumina Nanofluids, Journal of Nanoparticle Research, 11 (2009), pp. 1129-1136

[28] Huang, H., et al., A Sensitivity Analysis On Thermal Conductivity Of Al2O3-H2O Nanofluid: A Case Based On Molecular Dynamics And Support Vector Regression Method, Journal of Molecular Liquids, (2023), pp. 123652

[29] HUANG, H., et al., STUDY OF A NOVEL TERNARY SECOND-ORDER VISCOSITY MODEL ON Al 2 O 3-WATER NANOFLUID., Thermal Science, 27 (2023), pp. 4223-4234

[30] Grace, J.R., Ebneyamini, A., Connecting Particle Sphericity And Circularity, Particuology, 54 (2021), pp. 1-4

[31] Chamkha, A.J., On Laminar Hydromagnetic Mixed Convection Flow In A Vertical Channel With Symmetric And Asymmetric Wall Heating Conditions, International Journal of Heat and Mass Transfer, 45 (2002), pp. 2509-2525

[32] Chamkha, A.J., et al., FULLY DEVELOPED FREE CONVECTION OF A MICROPOLAR FLUID IN A VERTICAL CHANNEL, International Communications in Heat and Mass Transfer, 29 (2002), pp. 1119-1127

[33] Umavathi, J.C., et al., Unsteady Two-Fluid Flow And Heat Transfer In A Horizontal Channel, Heat and Mass Transfer, 42 (2005), pp. 81-90

[34] Chamkha, A.J., Flow Of Two-Immiscible Fluids In Porous And Nonporous Channels, Journal of Fluids Engineering-transactions of The Asme, 122 (2000), pp. 117-124

[35] Keimanesh, M., et al., Study Of A Third Grade Non-Newtonian Fluid Flow Between Two Parallel Plates Using The Multi-Step Differential Transform Method, Comput. Math. Appl., 62 (2011), pp. 2871-2891

[36] Qu, W., Mudawar, I., Experimental And Numerical Study Of Pressure Drop And Heat Transfer In A Single-Phase Micro-Channel Heat Sink, International Journal of Heat and Mass Transfer, 45 (2002), pp. 2549-2565

[37] Bashirnezhad, K., et al., Viscosity Of Nanofluids: A Review Of Recent Experimental Studies, International Communications in Heat & Mass Transfer, 73 (2016), apr., pp. 114-123

[38] Alawi, et al., Thermal Conductivity And Viscosity Models Of Metallic Oxides Nanofluids, International Journal of Heat and Mass Transfer, (2018)

Submitted: 16.10.2023.
Revised: 27.02.2024.
Accepted: 29.02.2024.